INTERNATIONAL JOURNAL FOR NUMERICAL METHODS IN FLUIDS
Int. J. Numer. Meth. Fluids **28**: 1371–1387 (1998)

NUMERICAL PREDICTION FOR LAMINAR FORCED CONVECTION HEAT TRANSFER IN PARALLEL-PLATE CHANNELS WITH STREAMWISE-PERIODIC ROD

ZHONG-XIAN YUAN, WEN-QUAN TAO* AND QIU-WANG WANG

School of Energy and Power Engineering, Xi'an Jiaotong University, Xi'an 710049, China

SUMMARY

A numerical study has been performed for the periodically fully-developed flow in two-dimensional channels with streamwise-periodic round disturbances on its two walls. To accurately describe the round disturbance boundary condition, a body fitted grid was used. The flow and heat transfer have been studied in the range of Reynolds number, $Re = 50–700$, and Prandtl number $Pr = 0.71$. The influences of disturbance parameters and Reynolds number on heat transfer and friction have been investigated in detail. Some of the solutions have been examined using both steady and unsteady finite difference schemes; and the same results have been obtained. The results show that different flow patterns can occur with different deployments of the disturbances. With appropriate configuration of the disturbances, the Nusselt number can reach a value four times greater than in a smooth channel at the same condition, with the penalty of a much greater pressure drop. On the other hand, if the disturbances are not deployed properly, augmentation of heat transfer cannot be acquired. © 1998 John Wiley & Sons, Ltd.

KEY WORDS: heat transfer; duct flow; laminar flow; boundary conditions

1. INTRODUCTION

Many duct configurations are employed in engineering to enhance heat transfer. There are numerous instances of ducts which have streamwise-periodic cross-sections. Many experimental studies have revealed that the entrance lengths of fluid flow and heat transfer for such streamwise-periodic ducts are much shorter than those of plain ducts, and quite often, three to five cycles can make the flow and heat transfer fully-developed [1–3]. More recently, one of the present authors has completed an experimental research project on the enhancement of internal duct heat transfer by periodically positioning longitudinal short rectangular fins on two principal walls [4]. To confirm the periodic fully-developed heat transfer characteristics, local wall temperatures were directly measured for each cycle using thermocouples and the two principal walls were electrically heated. In the Reynolds number range from 5×10^3 to 5.87×10^4, it is again revealed that after three to six cycles the local heat transfer coefficient distribution exhibits a periodic character, implying that both the fluid flow and heat transfer are in the periodic fully-developed region. This direct heat transfer measurement, along with

* Correspondence to: School of Engineering and Power Engineering, Xi'an Jiaotong University, Xi'an, Shaanxi 710049, China.

CCC 0271–2091/98/191371–17$17.50

Received November 1998
Accepted January 1998

those performed by previous authors using the naphthalene sublimation technique [1–3,5], definitely shows that for the configurations with streamwise-periodic cross-section, the fluid flow and heat transfer can be periodically fully-developed after passing a certain number of cycles. In engineering practice the streamwise length of such ducts is usually much longer than several cycles, therefore theoretical works for such ducts often focus on the periodically fully-developed fluid flow and heat transfer, which were first put forward and discussed in detail in Reference [6]. A channel mounted by roughness elements or ribs on its surfaces is one of the most important examples of streamwise-periodic ducts, and is widely used in the cooling of electronic equipment and gas turbine blades, as well as a high performance heat exchanger. A number of numerical simulations on the periodically fully-developed fluid flow and heat transfer characteristics have been performed [7–12]. The roughness elements or ribs studied in the existing publications are usually rectangular in shape, which does not provide any special difficulty for numerical simulation. However, sometimes elements may be round in shape [1,2], making the domain of one cycle irregular from the view point of numerical simulation. This difficulty can be solved by two methods. The first method is to approximate the curved walls by a succession of steps and extend the computation domain to a rectangle [7,10,13]. This method usually works well but may result in severe errors in some situations, especially for those cases having a drastically curved boundary. The other technique uses the body-fitted co-ordinates (BFC) to accommodate the irregular boundary [14]. This method has the advantages of good feasibility and high accuracy of numerical solution around the irregular boundary, and is adopted in the present study.

This paper is concerned with fluid flow and heat transfer characteristics in parallel-plate channels having streamwise-periodic round disturbances on its two principal walls (Figure 1). The fluid flow and heat transfer is considered to be laminar, two-dimensional and in steady state. As depicted in Figure 1, there are two dimensionless geometric parameters, i.e. P/E and H/E. In addition, the Prandtl number and Reynolds number must be included, resulting in a total of four parameters for the study of fully-developed characteristics. In this study, the Prandtl number was kept constant (0.71), while the other three parameters were varied in the following range: $P/E = 5$–20, $H/E = 3.33$–5, $Re = 50$–700. To accurately describe the round disturbance boundary condition, an algebraic grid generation technique [13] was adopted to generate a BFC system. A typical grid network for the computation domain, shown by the shaded area in Figure 1, is presented in Figure 2 for the case of $P/E = 7.5$ and $H/E = 5$.

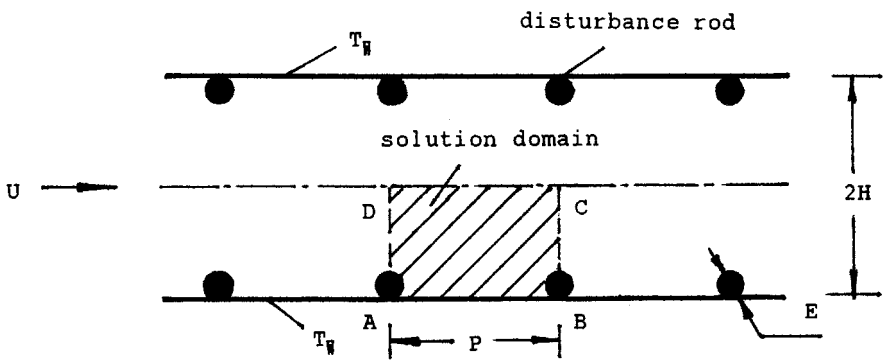

Figure 1. Diagram showing cycles of the periodic geometry.

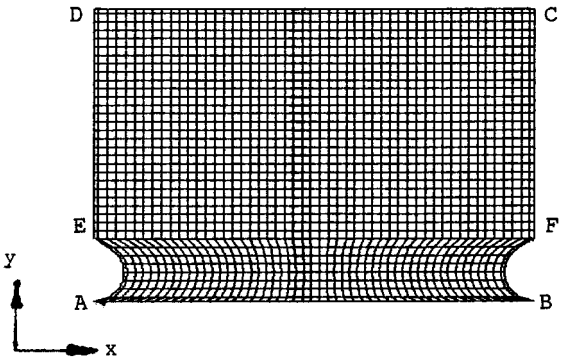

Figure 2. Representative grid system.

2. ANALYSIS

The identification of the periodicity characteristics of the velocity components and of a reduced pressure function enables the flow field analysis to be confined to a single isolated model, without involvement with the entrance region problem. For a uniform wall temperature boundary condition, which is the situation dealt with in the present study, dimensionless temperature profiles of similar shape also recur periodically. Thus, numerical analysis must only be conducted for a single module in the duct. Half of this module, *ABCD*, is indicated in Figure 1 to represent the solution domain because of the symmetric nature of the problem. For two-dimensional flow with constant properties, the governing equations are

$$\frac{\partial u}{\partial x}+\frac{\partial v}{\partial y}=0, \tag{1}$$

$$u\frac{\partial u}{\partial x}+v\frac{\partial u}{\partial y}=-\frac{1}{\rho}\frac{\partial p}{\partial x}+\nu\left(\frac{\partial^2 u}{\partial x^2}+\frac{\partial^2 u}{\partial y^2}\right), \tag{2}$$

$$u\frac{\partial v}{\partial x}+v\frac{\partial v}{\partial y}=-\frac{1}{\rho}\frac{\partial p}{\partial y}+\nu\left(\frac{\partial^2 v}{\partial x^2}+\frac{\partial^2 v}{\partial y^2}\right), \tag{3}$$

$$u\frac{\partial T}{\partial x}+v\frac{\partial T}{\partial y}=a\left(\frac{\partial^2 T}{\partial x^2}+\frac{\partial^2 T}{\partial y^2}\right). \tag{4}$$

Attention is now turned to the boundary conditions. For a periodically fully-developed flow the velocity components exhibit a periodic behavior:

$$u(0, y)=u(P, y), \tag{5}$$

$$v(0, y)=v(P, y), \tag{6}$$

and pressure can be subdivided into two components:

$$p(x, y)=-\beta x+p'(x, y), \tag{7}$$

where β is a constant representing the global pressure gradient, and the quantity p' is the periodic variable term with

$$p'(0, y)=p'(P, y). \tag{8}$$

The fluid temperature in the fully-developed periodic flow with a constant wall temperature does not simply repeat itself. But a properly defined dimensionless temperature, such as

$$\theta(x, y) = \frac{T(x, y) - T_w}{T_b(x) - T_w}, \tag{9}$$

where

$$T_b(x) - T_w = \frac{\int_A u(T - T_w)\, dA}{\int_A u\, dA}, \tag{10}$$

does have a periodic nature. So the inlet and outlet temperature boundary condition can be written as

$$\theta(0, y) = \theta(P, y). \tag{11}$$

Equations (5), (6), (8) and (11) describe the inlet and outlet boundary conditions. For both flow and heat transfer the top surface of the domain is a symmetry line, thus following equations are valid on it:

$$\frac{\partial u}{\partial y} = 0, \qquad \frac{\partial \theta}{\partial y} = 0, \qquad v = 0. \tag{12}$$

At the solid surfaces the no-slip requirement applies for velocity components, and a constant temperature is assigned to the bottom surface. The surface of the round disturbances is assumed to be adiabatic, which simulates inactive roughness elements in the experiments using the naphthalene sublimation technique [1,2].

There are two numerical algorithms used to solve the periodically fully-developed convective heat transfer problem. One algorithm was suggested in Reference [6]. In this algorithm, the dimensionless governing equation of temperature is transformed into an eigenvalue problem and the pressure term is replaced by the average pressure gradient β and the reduced pressure p'. The value of β is adjusted in the solution procedure to accommodate the algebraic equations. The other method implements the periodic conditions of Equations (5), (6) and (11) by mutual replacements of the field variables at inlet and outlet regions. This method was first adopted by Amano *et al.* [15,16] and later enhanced by Xin and Tao [9], Pang *et al.* [17] and Wang and Tao [18]. This algorithm seems to be more straightforward and easier to implement, therefore it will be adopted in the present work. For further details, Reference [18] may be consulted.

The finite volume approach was combined with the SIMPLE algorithm and the power-law scheme, in order to discretize and solve the governing equations. A careful check for the grid independence of the numerical solutions has been conducted to ensure the accuracy of the numerical solution. For this purpose, five grid systems 37×27, 57×32, 82×37, 120×60 and 150×80 were tested. For the case of $Re = 700$, $H/E = 5$, $P/E = 10$, the maximum relative deviation for Nusselt number between 82×37 and 150×72 is $< 4.5\%$. It was considered that the system of 82×37 nodes was a good compromise between necessary accuracy and efficiency (Figure 3), so it was used for majority of the geometry configurations except for the situation where $P/H = 1$, in which a 52×52 grid system was employed. It is generally considered that the power-law differential scheme (PLDS) may involve appreciable numerical diffusion, therefore a comparison of the present results with those obtained using other higher order schemes such as the central difference scheme (CDS) will be helpful to justify the present work.

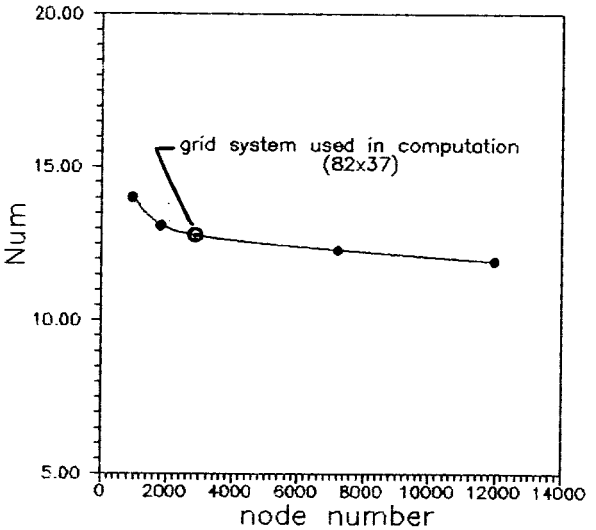

Figure 3. Grid-dependence character of Nu_m.

The comparative results are presented in Table I. It can be seen that for the problem studied, the difference between the results from PLDS and from CDS are negligible.

The numerical solution of transient governing equations does not necessarily converge to the solution of the steady state governing equations when the time approaches infinity, because this happens for the cases where bifurcation occurs [19]; therefore it is necessary to confirm that the numerical solutions are unique for the present study. Preliminary computations were performed for some typical cases using the transient governing equations. Steady state results obtained from the two sets of governing equations agree well with each other. For the case of $H/E = 5$, $P/E = 20$ and $Re = 700$, the relative deviation of the average Nusselt number is $< 3\%$, while that of the friction factor is even smaller ($\leq 10^{-2}$). In view of saving computer time, the steady method was adopted. The convergence criterion for terminating the iterative procedure is

$$G_{\text{res}} \leq 10^{-8}, \tag{13}$$

where G_{res} is the residual of the mass flow rate of the entire domain normalized by the mass flow rate at the inlet.

Table I. Comparison of results using PLDS and CDS

	Re	50	100	200	400	700
Nu	PLDS	7.811	8.166	8.988	10.648	12.776
	CDS	7.811	8.172	8.925	10.354	12.994
f	PLDS	2.3980	1.2197	0.6319	0.3352	0.1999
	CDS	2.3980	1.2198	0.6298	0.3329	0.2089

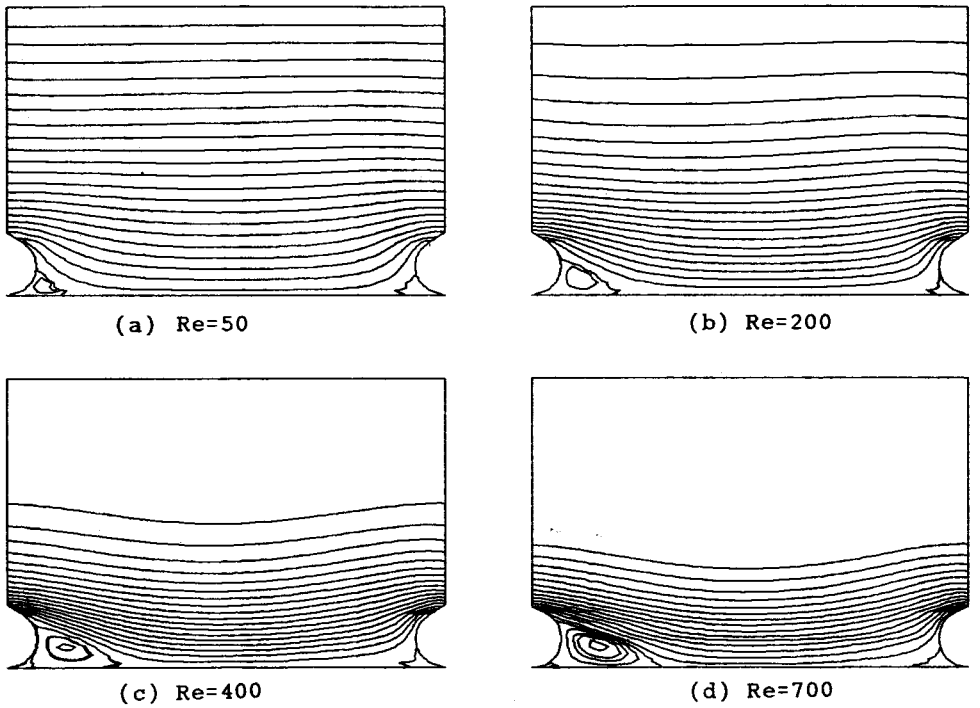

Figure 4. Flow patterns at different Reynolds numbers ($H/E = 5$, $P/E = 7.5$). (a) $Re = 50$; (b) $Re = 200$; (c) $Re = 400$; (d) $Re = 700$.

3. RESULTS AND DISCUSSION

The presentation of the numerical results will begin with the flow field, followed by an examination of the temperature field. The effects of P/E and H/E on the friction factor and heat transfer will then be discussed.

3.1. Results of flow field

Figure 4 shows the Reynolds number influence on the flow pattern for the case $H/E = 5$, $P/E = 7.5$. In order to show the flow in the vicinity of the rod clearly, the streamlines have not been drawn at a constant interval, with smaller intervals near the bottom wall. It can be seen from the flow pattern that the Reynolds number has a significant effect on the flow field. Apart from the global variation in flow pattern with Reynolds number, the special feature to be noted is the two vortices located in the upstream and downstream corners near the rods, and they can be seen in any of the four diagrams. For the very low Reynolds number case ($Re \leq 50$), the two vortices are almost identical and the flow streamlines are nearly symmetric about the mid-vertical line of the domain. With the increase in Reynolds number, the vortex behind the rod becomes larger, while the vortex ahead of the rod remains almost unchanged. Another notable feature of the vortex behind the rod is that its strength is also increased appreciably as the Reynolds number varies from 50 to 700. This will affect the local heat transfer distribution which will be discussed later.

The flow patterns for a higher P/E ($P/E = 20$) are shown in Figure 5, where the effect of Reynolds number can also be clearly observed.

3.2. Results of temperature field

Figure 6 represents the temperature fields for the case $H/E = 5$, $P/E = 10$. As expected, the increase in Reynolds number makes the isotherms cluster closer to the surface of the plate bottom. In addition, it can also be observed that in the near-wall region behind the left rod, the distribution of the isotherms is finer than that in the near-wall region ahead of the right rod, indicating different heat transfer intensity in the two regions.

As indicated earlier the rods were assumed to be adiabatic (a–r), hence, all of the isotherms in Figure 6 are normal to the rod surfaces. It is interesting to compare the results with those obtained using isothermal rods (i–r). Figure 7 provides isotherms for a channel with isothermal rods. In both sets of plots, the interval between two neighboring isotherm lines in Figures 6 and 7 was the same. It can be seen that, apart from the near-rod region, the isotherms in the near-wall region for the i–r case are not appreciably as fine as those for the a–r case under the same Reynolds number. This implies that the heat transfer process at the bottom of the i–r case is not as intensive as that of the a–r case.

3.3. Results of heat transfer and friction

Attention is now turned to the characteristics of heat transfer and friction. Before discussing the results, the definitions of the local Nusselt number, the average Nusselt number and the friction factor will be introduced.

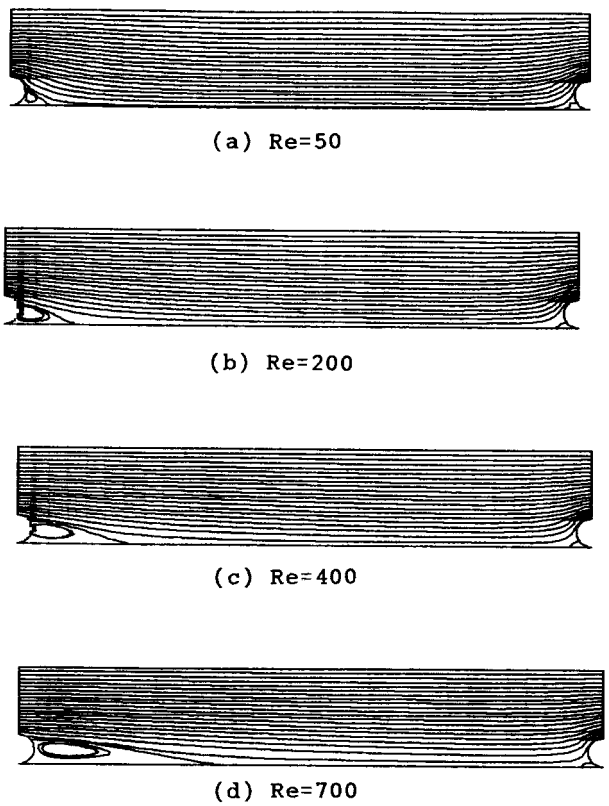

Figure 5. Flow patterns at different Reynolds numbers ($H/E = 3.33$, $P/E = 20$). (a) $Re = 50$; (b) $Re = 200$; (c) $Re = 400$; (d) $Re = 700$.

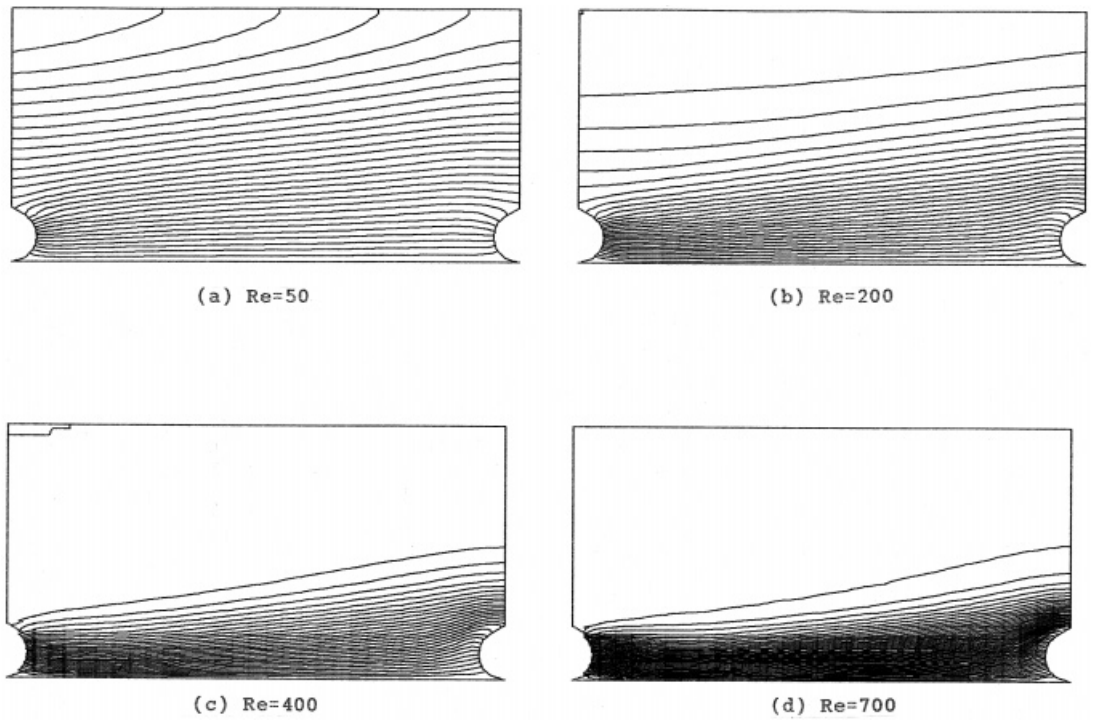

Figure 6. Temperature fields at different Reynolds numbers ($H/E = 5$, $P/E = 10$). (a) $Re = 50$; (b) $Re = 200$; (c) $Re = 400$; (d) $Re = 700$.

The local Nusselt number $Nu(x)$ takes the conventional definition,

$$Nu(x) = -\frac{k \cdot De}{T_b - T_w} \cdot \frac{\partial T(x, y)}{\partial y}\Big|_{y=0}, \tag{14}$$

and the average Nusselt number per cycle is defined as

$$Nu_m = \frac{1}{P} \int_0^P Nu(x)\, dx. \tag{15}$$

The Darcy definition is adopted for the friction factor:

$$f = \frac{(-dp/dx)De}{\frac{1}{2}\rho \bar{u}^2} = \frac{[\bar{p}(0) - \bar{p}(P)]De}{\frac{1}{2}\rho \bar{u}^2 P}, \tag{16}$$

where

$$\bar{p}(0) = \frac{1}{H - E} \int_E^H p(0, y)\, dy, \tag{17}$$

$$\bar{p}(P) = \frac{1}{H - E} \int_E^H p(P, y)\, dy. \tag{18}$$

In order to compare the friction factors of the present channels with those of the smooth parallel-plate duct at the same Reynolds number, the velocity used in Equation (16) is the average value in the middle of the cycle.

Typical distributions of the local Nusselt numbers are presented in Figure 8 for the case of $H/E = 5$, $P/E = 10$, 15, 20. In the figure the abscissa indicates the axial location, so the curve of $Nu(x)$–x represents the variation of the local heat transfer coefficients with the flow development in a periodically fully-developed cycle. $Nu(x)$ increases very quickly with x immediately after the left rod, reaches a maximum, and thereafter, gradually decreases. As approaching the right rod, $Nu(x)$ drops quickly and is near zero at the end of one cycle. The maximum of $Nu(x)$ corresponds to the reattachment point of the flow. One can also see that the relative distance P/E has a significant influence on the heat transfer of the surface. With the decrease of P/E the heat transfer is apparently enhanced. Figure 8(a,b,c) indicates that the effects of the Reynolds number on heat transfer become stronger at lower values of P/E. For a fixed P/E, the distributions of $Nu(x)$ change drastically with Reynolds number. The higher the Reynolds number, the larger $Nu(x)$, except for the vicinity of the rods, where the local Nusselt numbers at different Reynolds number cluster together. For each case, the local Nusselt number curve has a maximum. For a fixed geometric condition, the position of the maximum moves slightly downstream with the increase of Re. This may be attributed to the extension of the recirculating zone behind the rod with the Reynolds number (see Figure 4). It is interesting to note that the pattern of the local Nusselt number distribution curve predicted in this paper is quite similar to the test results presented in Reference [1], where experiments were conducted for the two-dimensional turbulent heat transfer in rod-roughened channels. The similarity between the distributions of the local Nusselt number of the present laminar flow predictions and the experimental turbulent results in Reference [1] gives support for the reliability of this numerical work.

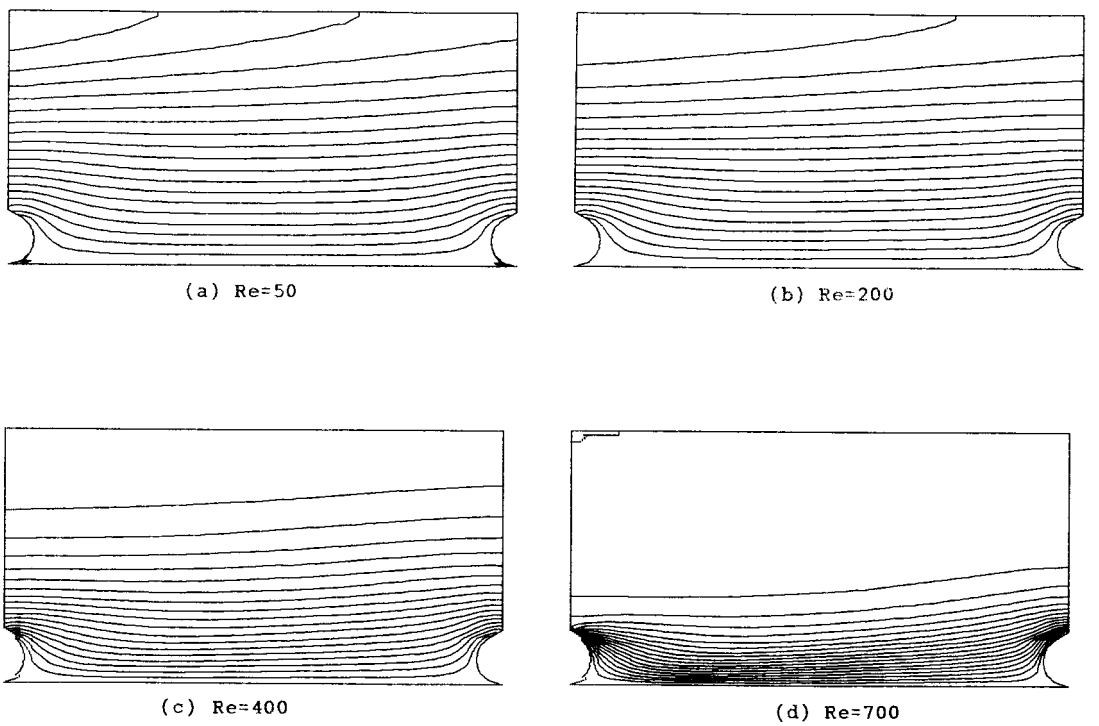

Figure 7. Temperature fields of roughened duct with isothermal disturbances ($H/E = 5$, $P/E = 10$). (a) $Re = 50$; (b) $Re = 200$; (c) $Re = 400$; (d) $Re = 700$.

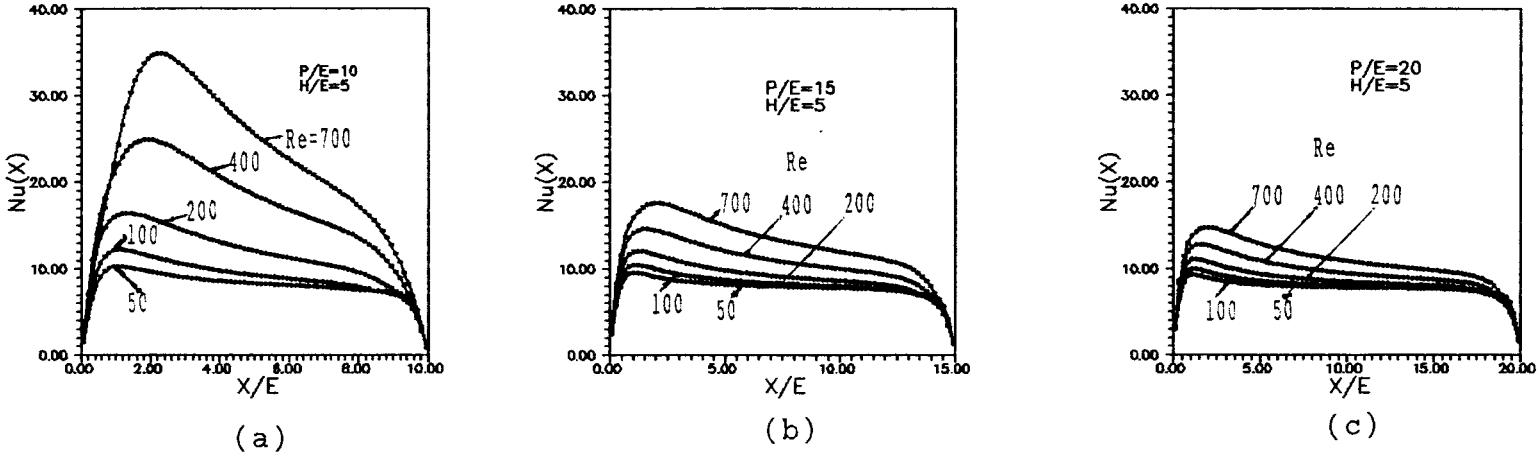

Figure 8. Distributions of local Nusselt number ($H/E = 5$). (a) $P/E = 10$; (b) $P/E = 15$; (c) $P/E = 20$.

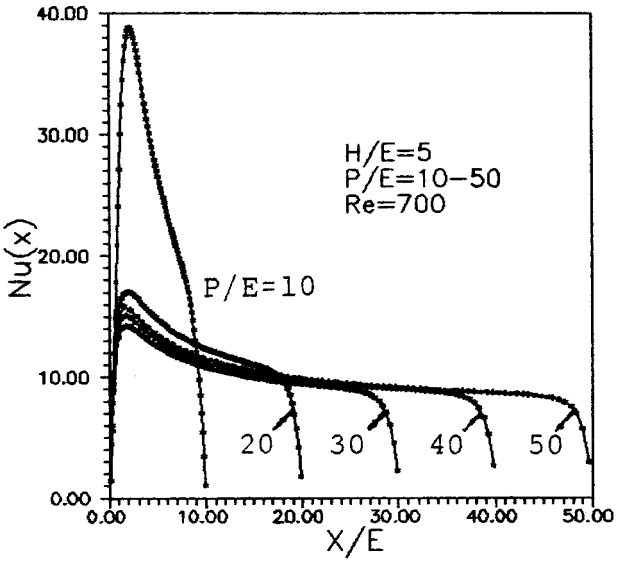

Figure 9. Influence of P/E on $Nu(x)$ ($H/E = 5$, $P/E = 10$–50).

Figures 9 and 10 represent the effects of P/E and H/E respectively, on the local Nusselt number at $Re = 700$. From these figures, the following two features may be noted. First, at a fixed value of H/E, the Nusselt number increases with the decrease in P/E. However, for the cases studied ($H/E = 5$, $P/E = 10$–50), the $Nu(x) \sim P/E$ dependency is very weak when $P/E > 20$. This is because when the distance between two neighboring rods is large enough, the existence of the second rod does not have appreciable affect on the flow pattern behind the first rod. Secondly, at a fixed P/E, the Nusselt number increases with the decrease in H/E. This is because the shortening of channel height relative to the rod makes the disruption effect of the rod to the flow field more significant, leading to a further enhancement of heat transfer.

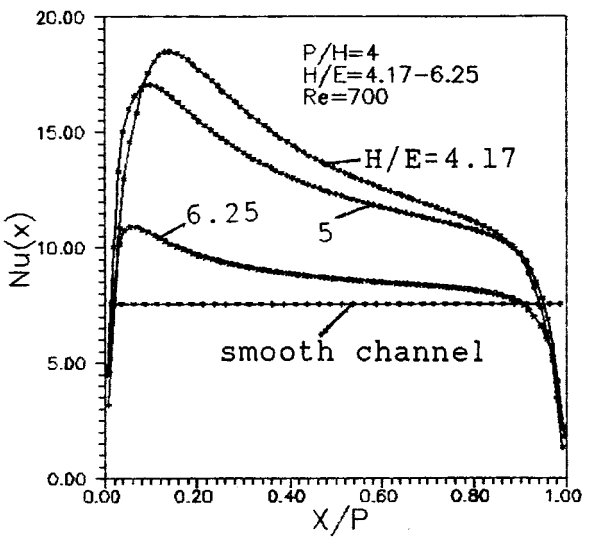

Figure 10. Influence of H/E on $Nu(x)$ ($H/E = 4.17$–6.25, $P/H = 4$).

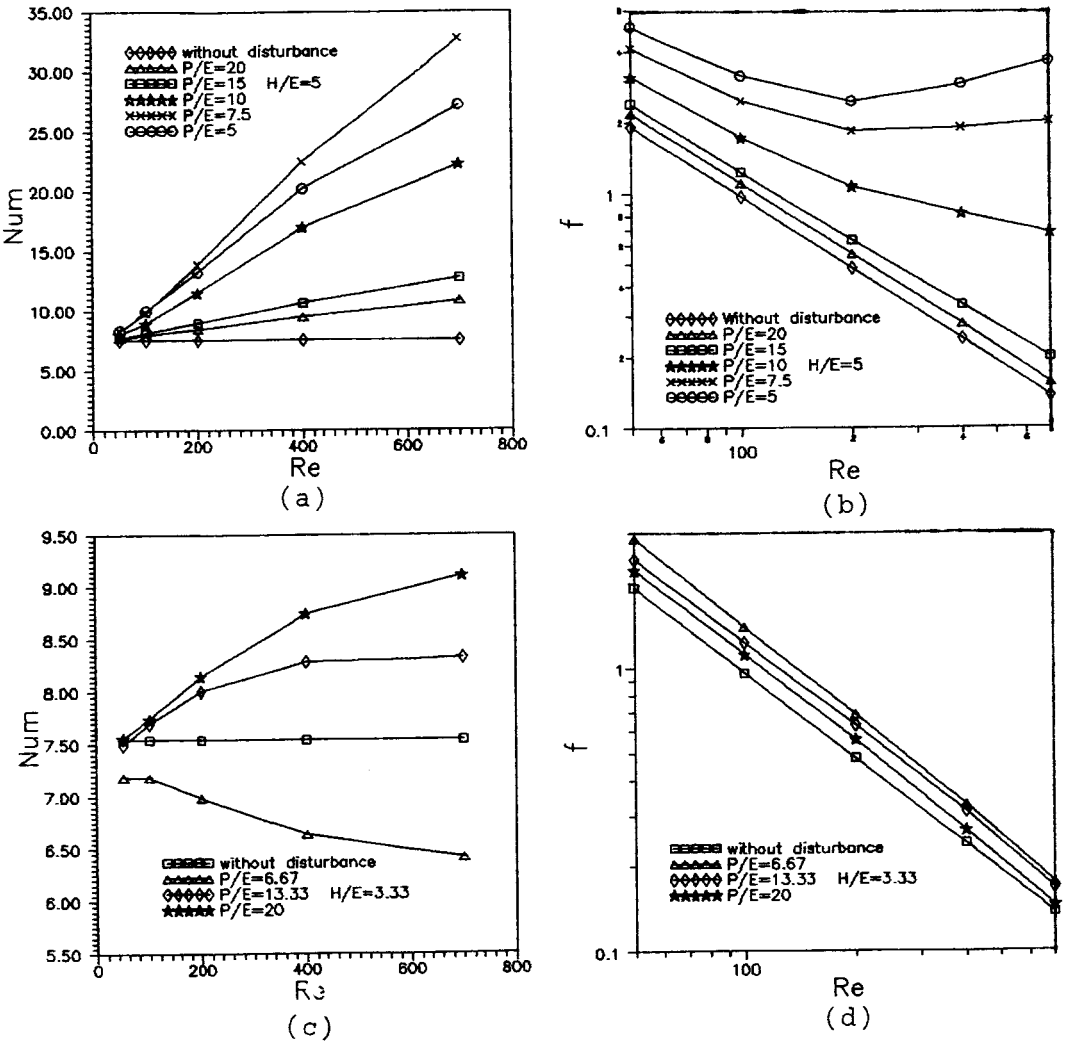

Figure 11. Per cycle average Nusselt number and friction factor ($Re = 50$–700). (a) $H/E = 5$; (b) $H/E = 5$; (c) $H/E = 3.33$; (d) $H/E = 3.33$.

Attention is now turned to the average heat transfer and the friction factor characteristics. The predicted results for cases of $H/E = 3.33$ and 5 are presented against Reynolds number in Figure 11, with P/E as parameter. For the situation of $H/E = 5$, heat transfer of the ducts with disturbances is augmented compared with that of smooth channels. As mentioned in the literature [6,7,9–11] the Nusselt number for the laminar channels with roughness elements depends strongly on Reynolds number, in contrast to the constant Nusselt number for the laminar flow in smooth channel. For the case of $H/E = 5$, $P/E = 7.5$ and $Re = 700$ the average Nusselt number, Nu_m, reaches more than 4-fold of the smooth channel's value 7.541. However, it can be seen from Figure 11(a) that for the five roughened cases, Nu_m approaches 7.541 when Re decreases. The results shown in Figure 11(c) for the case of $H/E = 3.33$ exhibit a somewhat more complex character. For $P/E = 20$ and 13.3 the results are similar to those in Figure 11(a). The result of $P/E = 6.67$ is quite different. Here, the heat transfer is not enhanced, rather, it

is attenuated. And as Re increases the extent of attenuation is accentuated. The reason for this is that at a higher relative height of the disturbance rods and smaller P/E, the recirculating region takes a large part of the plate surface, where the heat transfer is deteriorated because of the separation between the main flow and the wall surface. This trend is accentuated as Re increases (Figure 12). Thus, for the purpose of heat transfer enhancement, large relative height of the disturbance rods is not recommended. This type of character can also be observed from Figure 11(a), where for the case of $H/E = 5$, the variation of Nu_m with P/E is presented. It shows that from $P/E = 20$–7.5, heat transfer increases with the decrease of P/E, whereas Nu_m decreases as P/E approaches 5. Thus it can be inferred that for each value of H/E there exists a value of P/E at which the average Nusselt number reaches maximum.

As the Reynolds number definition is adopted the smooth plate-channel case, the variation of the friction factor for the ducts with disturbances presented in Figure 11(b,d) can be compared with that of corresponding smooth channel directly. Firstly, the friction factor in any case is higher than that of the smooth parallel channel at the same Re, as expected. The varying trend of f with Re shown in Figure 11(b) is quite similar to that provided in Reference [9], where the deviation of the friction factors between disturbed and smooth ducts usually becomes larger as Re increases. Whether the augmentation in heat transfer is attained or not, the pressure drop always increases with the decrease of P/E for a constant H/E. This is especially apparent for the case of $H/E = 3.33$, $P/E = 6.67$, where no heat transfer augmentation is obtained, while the corresponding friction factor line is located topmost (Figure 11(d)). It should be noted that despite the increase of Nu for most cases, the penalty in pressure drop is usually large. For example, for the case $H/E = 5$, $P/E = 7.5$ and $Re = 700$, the augmentation effect is about four times, and the pressure drop of the disturbed channel is about 20 times that of the smooth channel. The fact that the friction factor increases much faster than the increase in heat transfer by the presence of the disturbed rods requires that further analysis be performed to assess the net effect of the rods. This assessment will be made by comparing the enhanced ducts with a corresponding smooth plate channel. The comparison is carried out under the constraint of constant pumping power. As indicated in Reference [2], for fixed duct dimensions and equal thermophysical properties, the constraint of constant pumping power becomes

$$fRe^3 = (fRe^3)^*, \tag{19}$$

where the left-hand-side refers to the enhanced case, while the right-hand-side corresponds to the baseline case. This equation gives a relation between Re and Re^*. For a given value of

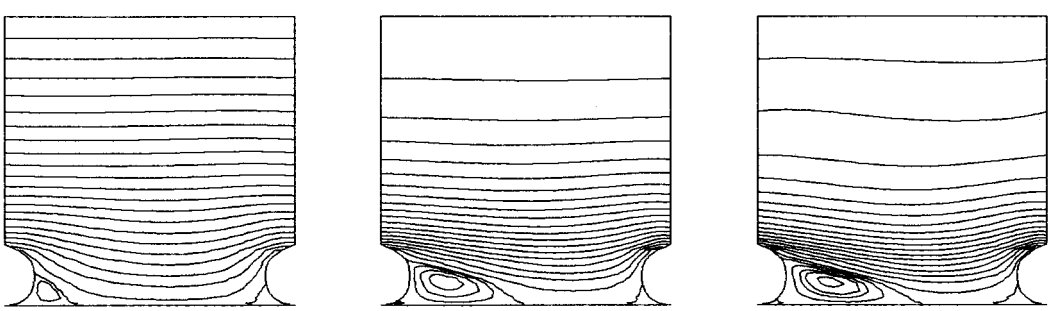

Figure 12. Effects of Reynolds number on the flow pattern.

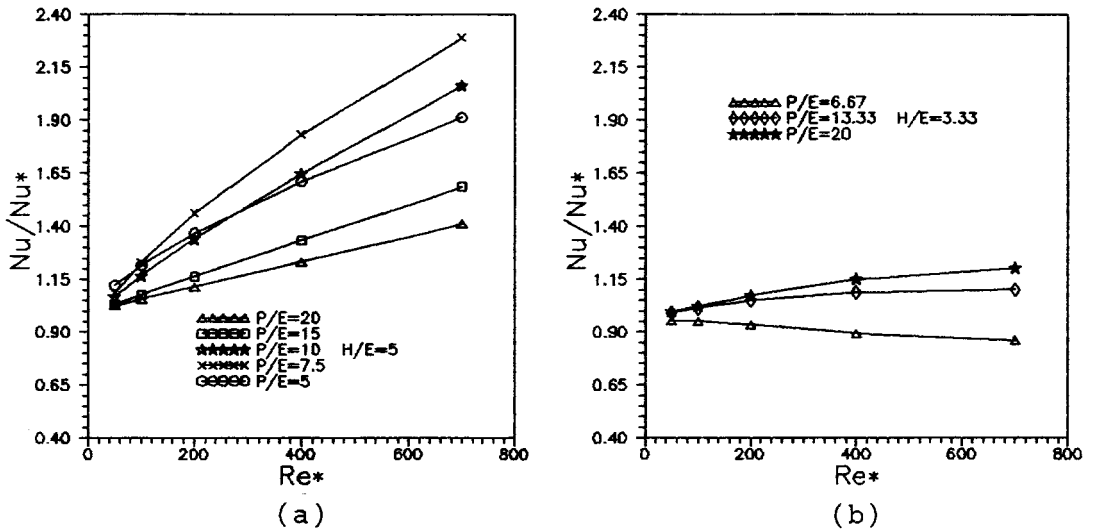

Figure 13. Heat transfer performance of roughened duct studied. (a) $H/E = 5$; (b) $H/E = 3.33$.

Re^*, the corresponding Re of a roughened duct may be obtained via iteration calculation using Equation (19).

The thermal performance of the roughened ducts is assessed by the relation of $Nu/Nu^* \sim Re^*$, where Nu^* is the Nusselt number for the baseline case and Nu corresponds to Re for the roughened case. The numerical results are presented in Figure 13. It can be seen that in the geometric parameter range studied, the largest value of Nu/Nu^* for the $H/E = 5$ duct is ≈ 2.3. For some other cases (e.g. $H/E = 3.33$, $P/E = 6.67$), the value of Nu/Nu^* is less than unity. Therefore it can be concluded that if the geometrical parameters are selected with care, the use of the periodic rod disturbances does provide some merit.

Finally the heat transfer characteristics of roughened ducts with isothermal disturbances will be discussed. The temperature fields at this condition have been described in Figure 7. The

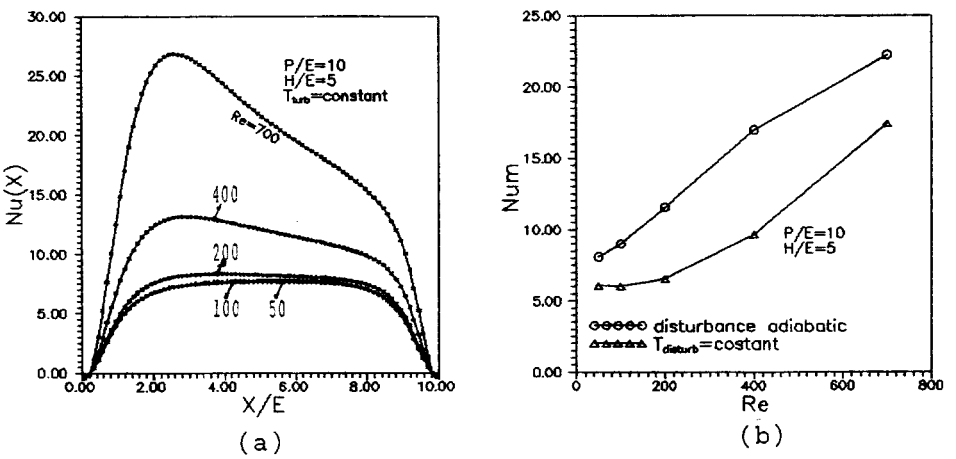

Figure 14. Local and average Nusselt number for duct with isothermal disturbances ($H/E = 5$, $P/E = 10$). (a) local; (b) average.

local and average Nusselt numbers are shown in Figure 14(a,b), respectively. Although the flow fields are identical, the distributions of $Nu(x)$ shown in Figure 14(a) and Figure 8(a) are apparently different. The major difference lies in the fact that the maximum $Nu(x)$ in Figure 14(a) is smaller than the corresponding one in Figure 8(a). In addition, with the decrease in Reynolds number, the peaks on the $Nu(x)$ curve gradually disappear for the isothermal case. The per cycle average Nusselt numbers for the two rod thermal boundary conditions also exhibit a large difference (Figure 14(b)). The average Nusselt number for the adiabatic case is always greater than the isothermal one, and for $Re = 400$, the difference is as large as 40%. It should be noted that in order to keep the comparison at an equal level, when calculating the Nusselt number for the i–r case, the heat transfer across the rod surface is not taken into account. When $Re < 250$, the value of Nu_m for the isothermal case is < 7.541, the value of Nusselt number for a smooth parallel-plate channel in fully developed region. This is quite different to the turbulent flow case, for which both experiments [20,21] and numerical computations [22] have shown that the rod boundary thermal condition does not have a significant effect on the per cycle average Nusselt number.

4. CONCLUSIONS

The fully developed laminar flow and heat transfer in parallel-plate channels with adiabatic streamwise-periodic rod disturbances have been investigated numerically using the BFC technique. The influences of P/E, H/E and Re on the flow and heat transfer characteristics have been studied with Prandtl number equal to 0.71.

Thermal performance of the roughened ducts has been assessed by comparing them with the smooth parallel-plate channel with the constraint of constant pumping power. A brief comparison between the cases of adiabatic rods and isothermal rods has also been made.

The distribution pattern of the local Nusselt number is quite similar to that of experimental turbulent flow results found in the literature. In the range of $Re = 50$–700, the appropriate geometric parameters P/E and H/E range respectively, from eight to 20 and from four to five, where the ratio of Nu/Nu^* varies from 1.04 to 2.29. The thermal boundary condition of the rods has an appreciable effect on the per cycle average Nusselt number, and the case of adiabatic rods gives a higher value of the Nusselt number.

ACKNOWLEDGMENTS

This work was supported by the Doctorate Fund of the Chinese Universities and Institutes and the National Natural Science Foundation of China.

APPENDIX A. NOMENCLATURE

a	air thermal diffusion coefficient
A	sectional area
De	equivalent diameter of duct
E	diameter of the rod disturbance
f	friction factor
G_{res}	convergence criterion
H	half height of the duct

k air thermal conductivity
Nu Nusselt number
p fluid pressure
P pitch of the rod disturbance
p' pressure periodic variable
Pr Prandtl number
Re Reynolds number
T fluid temperature
T_b sectional bulk temperature
T_w wall temperature
u, v velocity components
x, y Cartesian co-ordinates

Greek symbols

β cycle mean pressure gradient
ϕ representative of u, v or T
v air viscosity coefficient
θ dimensionless temperature
ρ air density

Subscripts

m mean value
$*$ baseline case

REFERENCES

1. E.M. Sparrow and W.Q. Tao, 'Enhanced heat transfer in a flat rectangular duct with streamwise-periodic disturbances at one principal wall', *ASME J. Heat Transf.*, **105**, 851–861 (1983).
2. E.M. Sparrow and W.Q. Tao, 'Symmetric vs asymmetric periodic disturbances at the walls of heated flow passage', *Int. J. Heat Mass Transf.*, **27**, 2133–2144 (1984).
3. S.S. Lue, H.Z. Huang and W.Q. Tao, 'Experimental study on heat transfer and pressure drop characteristics in developing region for arrays of obliquely positioned plates of non-uniform length', *Exp. Therm. Fluid Sci.*, **7**, 30–38 (1993).
4. Z.X. Yuan, 'Investigations on new enhancement structures for duct heat transfer and impingement cooling for gas turbine blades', *Ph.D Thesis*, Xi'an Jiaotong University, China, 1997.
5. H.Z. Huang and W.Q. Tao, 'An experimental study on heat and mass transfer and pressure drop characteristics for arrays of nonuniform plate length positioned obliquely to the flow direction', *ASME J. Heat Transf.*, **115**, 568–575 (1993).
6. S.V. Patanker, C.H. Liu and E.M. Sparrow, 'Fully developed flow and heat transfer in ducts having streamwise-periodic variations of cross-sectional area', *ASME J. Heat Transf.*, **99**, 180–186 (1977).
7. E.M. Sparrow and A.T. Prata, 'Numerical solutions for laminar flow and heat transfer in a periodically converging-diverging tube, with experimental confirmation', *Numer. Heat Transf.*, **6**, 441–461 (1983).
8. Y.-J. Hong, S.-S. Hsieh and H.-j. Shih, 'Numerical computation of laminar separation and reattachment of flow over surface-mounted ribs', *ASME J. Fluids Eng.*, **113**, 190–198 (1991).
9. R.C. Xin and W.Q. Tao, 'Numerical prediction of laminar flow and heat transfer in wavy channels of uniform cross-sectional area', *Numer. Heat Transf.*, **14**, 465–481 (1988).
10. A.T. Prata and E.M. Sparrow, 'Heat transfer and fluid flow characteristics for an annulus of periodically varying cross section', *Numer. Heat Transf.*, **8**, 285–304 (1984).
11. C.-H. Chang and W.-H. Huang, 'Numerical prediction for laminar forced convention in parallel-plate channels with transverse fin arrays', *Int. J. Heat Mass Transf.*, **34**, 2739–2749 (1991).
12. K.M. Kelkar and S.V. Patankar, 'Numerical prediction of flow and heat transfer in a parallel plate channel with staggered fins', *ASME J. Heat Transf.*, **109**, 25–30 (1987).
13. W.Q. Tao, *Numerical Heat Transfer*, Xi'an Jiaotong University Press, Xi'an, China, 1988.
14. J.R. Thompson, Z.U.A. Warsi and C.W. Martin, *Numerical Grid Generation, Foundations and Applications*, North-Holland, New York, 1985.

15. R.S. Amano, 'A numerical study of laminar and turbulent heat transfer in a periodically corrugated wall channel', *ASME J. Heat Transf.*, **107**, 564–569 (1985).
16. R.S. Amano, A. Bag Herlee, R.J. Smith and T.G. Niss, 'Turbulent heat transfer in a corrugated-wall channel with and without fins', *ASME J. Heat Transf.*, **109**, 62–67 (1987).
17. K. Pang, W.Q. Tao and H.H. Zhang, 'Numerical analysis of fully developed fluid flow and heat transfer for arrays of interrupted plates positioned covergently–divergently along the flow direction', *Numer. Heat Transf.*, **18**, 305–324 (1990).
18. L.B. Wang and W.Q. Tao, 'Heat transfer and fluid flow characteristics of plate-array aligned at angles to the flow direction', *Int, J. Heat Mass Transf.*, **38**, 3053–3063 (1995).
19. F. Durst, J.C.F. Pereira and C. Tropea, 'The plane symmetric sudden-expansion flow at low Reynolds numbers', *J. Fluid Mech.*, **248**, 567–581 (1993).
20. R.J. Boyle, 'Heat transfer in serpentine passage with turbulence promoters', *ASME Paper*, *No. 84-HT-24.*
21. J.C. Han and P. Hang, 'Effect of rib angle orientation on local mass transfer distribution in a three-pass rib-roughened channel', *ASME J. Turbomach.*, **113**, 123–129 (1991).
22. C.Y. Zhao and W.Q. Tao, 'A three-dimensional investigation of turbulent flow and heat transfer in a rectangular channel with a sharp 180-degree turn in two-pass rib-roughened channels', *Int. Comm. Heat Mass Transf.*, **24**, 587–596 (1997).

